1   **Dark nanodiscs as a model membrane for evaluating membrane protein thermostability by**

2   **differential scanning fluorimetry.**

3   Jazlyn A. Selvasingh[1,2], Eli Fritz McDonald[1,2], Jacob R. Mckinney[1,2], Jens Meiler[1,2,3]*, Kaitlyn V. Ledwitch[1,2,4]*

4

5   [1]Center for Structural Biology, Vanderbilt University, Nashville, TN 37240, USA

6   [2]Department of Chemistry, Vanderbilt University, Nashville, TN 37235, USA

7   [3]Institute of Drug Discovery, Faculty of Medicine, University of Leipzig, 04103 Leipzig, Germany

8   [4]Lead contact

9

10 *To whom the correspondence should be addressed: Kaitlyn Ledwitch, Department of Chemistry, Vanderbilt

11 University, Center for Structural Biology, MRBIII 5154E, Nashville, TN 37232. Telephone: (229) 412-0214. Fax:

12 (615) 936-2211. E-mail: k.ledwitch@vanderbilt.edu.

13

14 *To whom the correspondence should be addressed: Jens Meiler, Department of Chemistry, Vanderbilt

15 University, Nashville TN 37232, Institute for Drug Discovery, Leipzig University, 04103 Leipzig, Germany. E-

16 mail: jens@meilerlab.org. Telephone: +1 (615) 936-5662.

17

18 **Abstract**

19   Measuring protein thermostability provides valuable information on the biophysical rules that govern

20 structure-energy relationships of proteins. However, such measurements remain a challenge for membrane

21 proteins. Here, we introduce a new experimental system to evaluate membrane protein thermostability. This

22 system leverages a recently-developed non-fluorescent membrane scaffold protein (MSP) to reconstitute

23 proteins into nanodiscs and is coupled with a nano-format of differential scanning fluorimetry (nanoDSF). This

24 approach offers a label-free and direct measurement of the intrinsic tryptophan fluorescence of the membrane

25 protein as it unfolds in solution without signal interference from the "dark" nanodisc. In this work, we demonstrate

26 the application of this method using the disulfide bond formation protein B (DsbB) as a test membrane protein.

27 NanoDSF measurements of DsbB reconstituted in dark nanodiscs show a complex biphasic thermal unfolding

28 pattern in the presence of lipids with a minor unfolding transition followed by a major transition. The inflection

29 points of the thermal denaturation curve reveal two distinct unfolding midpoint melting temperatures (T_m) of 70.5

30 °C and 77.5 °C, consistent with a three-state unfolding model. Further, we show that the catalytically conserved

31 disulfide bond between residues C41 and C130 drives the intermediate state of the unfolding pathway for DsbB

32 in a nanodisc. We introduce this method as a new tool that can be used to understand how compositionally, and

33 biophysically complex lipid environments drive membrane protein stability.

34

35 **Keywords:** integral membrane protein, melting temperature, dark nanodiscs, nano-format differential scanning

36 fluorimetry (nanoDSF), thermostability

Introduction

Membrane proteins represent a class of proteins that are challenging targets for biophysical studies because they associate with unique asymmetric lipid environments. Evaluating the thermal stability of membrane proteins relies on spectroscopic or calorimetric assays that perform well and are robust for water-soluble proteins such as circular dichroism (CD)[1], differential scanning calorimetry (DSC)[2], and differential scanning fluorimetry (DSF)[3]. These tools often fall short for membrane proteins because they require a model membrane system for *in vitro* studies, which often convolute the signal and measurement. Detergent micelles are the most widely used model membrane systems for biophysical studies, despite their known effect on membrane protein structure, stability, and function[4,5]. To date, few studies tabulated in the membrane protein thermodynamic database (MPTherm) report thermostability measurements for membrane proteins in the presence of lipids[6] despite the key role lipids play in thermal stability[7-9]. This is largely due to technical hurdles associated with developing simple tools to investigate the effects of lipids on membrane protein stability.

Model membrane systems used for membrane protein stability measurements range from micelles and bicelles to more native-like systems such as nanodiscs[10], saposin-derived lipid nanoparticles[11], styrene-maleic acid copolymers[12], and proteoliposomes[13]. Many sophisticated attempts have been made to evaluate how lipids impact membrane protein stability using a variety of approaches. For example, an ion mobility mass spectrometry approach showed that specific lipid types increased protein unfolding resistance for several membrane protein systems when compared to micelle conditions alone[14]. Nji *et al.* developed a thermal shift assay to probe the effect of lipid interactions on membrane protein stability[15]. That work revealed that cardiolipin increased the thermal stability of a sodium–proton antiporter when added to the detergent-solubilized membrane protein sample. Treuheit *et al.* was the first to study the thermal stability of a membrane-associated protein, cytochrome P4503A4 (CYP3A4), in a nanodisc by DSC[16]. The results showed an increase in the thermal stabilization of CYP3A4 incorporated into nanodiscs compared to an aggregated state in solution. Flayhan *et al.* tested the use of saposin lipid nanoparticles (SapNPs) as a model membrane system for membrane protein reconstitutions[17]. Three different membrane protein systems were reconstituted in SapNPs, two integral membrane peptide transporters (DtpA and PepT) and the small-conductance mechanosensitive channel T2, for thermostability measurements by nano-format of differential scanning fluorimetry (nanoDSF). All three membrane protein test systems revealed an increase in thermal stabilization (i.e., melting temperature) in SapNPs compared to n-dodecyl-β-D-maltoside (DDM) micelles. These attempts suggest we still lack robust tools for evaluating and quantitatively comparing how lipids regulate the structure and stability of membrane proteins.

Recently, a membrane scaffold protein (MSP) construct was engineered that replaces all tryptophan and tyrosine residues with phenylalanine for reconstituting membrane proteins in nanodiscs making them fluorescently dark[18]. Nanodiscs are attractive systems because the lipid composition can be precisely controlled and therefore, can be used as a model membrane to systematically dissect the effect of lipid types on membrane protein thermal stability. In this work, we introduce a new method that couples the non-fluorescent MSP to form dark nanodiscs with nanoDSF measurements of intrinsic tryptophan fluorescence. This offers a facile

2

measurement of the thermal unfolding of reconstituted membrane proteins without signal interference from the nanodisc. Further, thermostability measurements by nanoDSF offer many advantages in that it is a label-free approach that monitors the shift in intrinsic tryptophan fluorescence as the protein unfolds and does not require a high sample consumption. We test the utility of this approach using the *E. coli* disulfide bond formation protein B (DsbB) as a model membrane protein system. The topology of DsbB is shown in **Figure 1** and consists of four transmembrane domains (TMD1–TMD4) with a catalytically-conserved interloop disulfide bond that plays an important part in the reaction cycle[19]. We use this as a model membrane protein because the thermodynamic behavior of DsbB has been extensively evaluated under chemical denaturation conditions making it an ideal test system for comparison[20,21].

Early studies by Otzen *et al.* combined fluorescence-based stopped-flow kinetic experiments and chemical denaturation in sodium dodecyl sulfate and dodecyl maltoside (SDS-DM) mixed micelles to study the unfolding/refolding of DsbB. These experiments revealed a three-state unfolding model for DsbB consisting of the native state in DM, an unfolding intermediate, and the SDS-denatured state[20]. The authors also performed the same experiments under reducing conditions to investigate the role disulfide bonds play in the stability of DsbB. They showed that under reducing conditions unfolding rate constants increased and that the disulfide bonds contribute to the stability of the protein. Regardless, it remains unclear if the observed intermediate state in SDS-DM mixed micelles is biophysically-relevant. In this work, we report nanoDSF thermostability data for DsbB reconstituted in our dark nanodiscs to showcase the utility of our method. Our data suggests DsbB undergoes a three-state/biphasic unfolding process in dark nanodiscs. We compare these results to a panel of different detergent micelle conditions and under conditions where the C41-C130 interloop disulfide bond is disrupted by reducing conditions.

Results

The thermal unfolding curve for DsbB reconstituted in a dark nanodisc follows a biphasic unfolding pattern with a minor transition followed by a second major transition.

One of the most widely used proxies for overall protein stability is thermostability. We reconstituted DsbB in dark nanodiscs loaded with a 3:2 molar ratio of 1,2-dimyristoyl-sn-glycero-3-phosphocholine (DMPC) and 1,2-dimyristoyl-sn-glycero-3-phosphorylglycerol (DMPG) lipids and measured the thermostability of the protein by nanoDSF. **Figure 2A** shows the intrinsic tryptophan fluorescence ratio at 350 and 330 nm for DsbB (F350/F330 ratio) over a thermal ramp from 25 °C to 95 °C. The inflection points of the unfolding curve determined from the experimental derivative correspond to the unfolding midpoint melting temperatures (T_m). **Figure 2B** shows the first derivative of the F350/F330 ratio as a function of temperature. **Figure 2C** shows a representative SDS-PAGE gel demonstrating sample purity following a reconstitution reaction for DsbB in a dark nanodisc. The experimental derivative of the unfolding curve reveals two distinct T_m values of 70.5 °C and 77.5 °C. These results suggest that DsbB in a nanodisc follows a three-state/biphasic unfolding model: native (**N**) → intermediate (**I**) → unfolded (**U**). To confirm that the nanodisc does not contribute to the three-state/biphasic unfolding

3

110   mechanism, we performed nanoDSF measurements on empty dark nanodiscs (i.e., in the absence of protein)

111   loaded with the same lipid content. Indeed, the dark nanodisc itself is fluorescently undetectable over the

112   temperature gradient (**Figure 2A, grey line**). This can be compared to the results for empty nanodiscs prepared

113   using conventional (fluorescent) MSPs (**Figure 3A-B**). The near-baseline signal for the empty dark nanodisc

114   sample up to roughly 85 °C suggests that the engineered MSP used for reconstitutions does not interfere with

115   the signal observed for the target DsbB protein. Furthermore, DMPC and DMPG lipids have melting

116   temperatures below the range of the thermal gradient measured (i.e., below 25 °C) and both are cylindrical lipids

117   that lack the required geometry for a transition to a hexagonal or inverted hexagonal phase[22]. Therefore, we do

118   not expect that the phase transition of the lipids used in this work contributes to the unfolding transitions observed

119   for DsbB. We also report the fraction unfolded curves (baseline corrected) for visualization of the T_m values at

120   the inflection point which is shown in **Figure S1A-D**. We also report the dynamic light scattering measurements

121   collected in **Figure S2A-E (third row)** as a cumulative radius plot to evaluate any contributions of aggregation

122   to our unfolding curve data.

123

124   **The thermal unfolding curves for DsbB under a panel of detergent micelle conditions each show a major**

125   **unfolding transition and decreased T_m values compared to nanodiscs.**

126   We selected a range of detergents with different physiochemical properties and hydrocarbon chain

127   lengths to compare the thermostability of DsbB in nanodiscs to different micelle conditions. **Figure S3A-E (first**

128   **row)** shows the F350/F330 ratio for the unfolding curves for detergent-solubilized DsbB in DDM, lauryl maltose

129   neopentyl glycol (LMNG), n-decyl-β-maltoside (DM), lauryldimethylamine oxide (LDAO), and lyso-

130   myristoylphosphatidylglycerol (LMPG) micelles. **Figure S3A-E (second row)** shows the respective experimental

131   derivative plots for the unfolding curves under each detergent micelle condition revealing a single major inflection

132   point corresponding to a single T_m value. Detergent-solubilized DsbB switches to a single major unfolding

133   transition in the case of DDM and LMPG micelles. A second less-defined peak can be seen towards the end of

134   the thermal gradient, roughly 40 °C above the first transition, for DsbB under LMNG, DM, and LDAO conditions.

135   The measured thermostability for DsbB in detergent micelles from most stable to least stable is DDM > LMPG >

136   LMNG > DM > LDAO. The fraction unfolded curves (baseline corrected) for each detergent condition are reported

137   in **Figure S4** for visualization of the T_m values at the inflection point as well as the dynamic light scattering data

138   collected as a cumulative radius plot in **Figure S3A-E (third row)**.

139

140   **The experimentally determined T_m value for the fluorescent MSP-based nanodisc is well outside the**

141   **range of T_m values observed for DsbB.**

142   We also tested the thermostability of a fluorescent MSP-based nanodisc to ensure that it was not

143   contributing to the three-state/biphasic unfolding pattern observed for DsbB. **Figure 3A** shows the F350/F330

144   ratio for the unfolding curve for a fluorescent MSP-based nanodisc in the absence of DsbB. **Figure 3B** shows

145   the respective experimental derivative plot for the unfolding curve. The inflection point corresponds to a T_m value

4

146 of 86.6 °C, which is more than 10 °C above the melting temperatures observed for DsbB in a dark nanodisc (see

147 – **Figure 2B**). **Figure S1B** shows the fraction unfolded curve (baseline corrected) for the fluorescent MSP-based

148 nanodisc for visualization of the T_m value at the inflection point. This data illustrates that the baseline DSF trace

149 from fluorescent nanodiscs would be problematic had these nanodiscs been used for this study of DsbB. The

150 dynamic light scattering data collected for the empty fluorescent nanodiscs is shown in **Figure S2C (third row)**

151 as a cumulative radius plot indicating that aggregation of the empty fluorescent nanodiscs falls outside the range

152 of T_m values observed for DsbB in the dark nanodisc.

153

154 **The engineered *dark loop* DsbB construct does not appear to change the three-state /biphasic unfolding**

155 **pattern for DsbB but displays higher transition temperatures.**

156 Otzen *et al.* reported that a single exponential for both the kinetic folding and unfolding of DsbB in mixed

157 micelles was observed suggesting that DsbB refolds/unfolds as a single cooperative unit with a strong coupling

158 between the four transmembrane domains and periplasmic loop regions[20]. We were interested in determining if

159 this cooperativity of unfolding was specific to detergent conditions considering that our thermostability

160 measurements of DsbB in a nanodisc revealed a biphasic unfolding pattern. We hypothesized that under

161 nanodisc conditions, the three-state/biphasic pattern was the result of the extramembrane loop region unfolding

162 independent of the transmembrane core. To test this hypothesis, we engineered a *dark loop* DsbB construct

163 where the Trp residues in the 46-residue extracellular loop region were mutated out to spectroscopically silence

164 this region of the protein (i.e., W113F, W119L, and W135F). **Figure S5A** shows the F350/F330 ratio for the

165 unfolding curve for the *dark loop* construct assembled in a dark nanodisc. **Figure S5B** shows the respective

166 experimental derivative plot for the unfolding curve revealing two inflection points at 85.3 °C and 91.7 °C. Indeed,

167 nanoDSF measurements of *dark loop* DsbB reconstituted in a dark nanodisc showed that the protein still

168 undergoes a three-state/biphasic unfolding process, consistent with the fact that DsbB unfolds as a cooperative

169 unit (see – **Figure S5**). This observation further supports that an early unfolding of the periplasmic loop regions

170 is not a contributing factor to the observed biphasic unfolding pattern. However, we note the melting temperatures

171 observed for the *dark loop* construct are near or above those observed for the empty fluorescent nanodisc (i.e.,

172 86.6 °C). **Figure S1C** shows the fraction unfolded curve (baseline corrected) for the *dark loop* DsbB construct

173 reconstituted in a nanodisc for visualization of the T_m value at the inflection point. Additionally, we report the

174 dynamic light scattering data that we collected for the *dark loop* DsbB construct in dark nanodiscs as a cumulative

175 radius plot in **Figure S2E (third row)**.

176

177 **The thermal unfolding mechanism for DsbB measured under reducing conditions shifts the unfolding**

178 **curve from three-state/biphasic to two-state/monophasic.**

179 We purified wild-type DsbB under reducing conditions (i.e., the addition of 2 mM TCEP) to test the

180 hypothesis that the interloop disulfide bond between cysteine residues C41 and C130 plays a key role in the

181 formation of the intermediate unfolding state. **Figure 4A** shows the F350/F330 ratio for the unfolding curve for

182 C41-C130 reduced DsbB assembled in a dark nanodisc. **Figure 4B** shows the respective first derivative plot for

183 the unfolding curve revealing a single inflection point corresponding to a T_m value of 76.6 °C, which is within the

184 range of the T_{m2} value observed for DsbB under non-reducing conditions. This suggests that the intermediate

185 unfolding state observed for DsbB is mediated by the C41-C130 disulfide bond. More interestingly, this distinct

186 three-state/biphasic unfolding pattern is not observed under detergent conditions further suggesting that this

187 interloop disulfide bond intermediate state is mediated by the presence of lipids. **Figure S1D** shows the fraction

188 unfolded curve (baseline corrected) for C41-C130 reduced DsbB reconstituted in a nanodisc for visualization of

189 the T_m value at the inflection point and **Figure S2B (third row)** shows dynamic light scattering data collected for

190 DsbB under reducing conditions in a dark nanodisc as a cumulative radius plot.

191

Discussion

193 **The intermediate minor transition state observed for the thermal unfolding of DsbB in a dark nanodisc**

194 **is absent under detergent micelle conditions.**

195   Tools to evaluate membrane protein stability in the presence of lipids or a lipid-based model membrane

196 system remain a technical challenge and are often reverted to studies in detergent micelles. We describe in this

197 work the development and evaluation of dark nanodiscs as a model membrane system for nanoDSF

198 thermostability measurements. We present this as a new tool that can be used to evaluate how lipid-protein

199 interactions regulate membrane protein stability. We show that the dark nanodiscs are fluorescently undetectable

200 by nanoDSF, making them an ideal model membrane system to investigate the effect of lipids and specific lipid

201 types on membrane protein thermostability.

202   We observed that DsbB reconstituted in a dark nanodisc follows a three-state/biphasic thermal unfolding

203 model that can be described in terms of a native state (**N**), an intermediate state (**I**), and an unfolded state (**U**).

204 **Figure 5** depicts the assembled DsbB-dark nanodisc complex as it unfolds along the thermal gradient. In this

205 model, the DsbB thermal unfolding curve does not reach a plateau (see – **Figure 2A**) suggesting that residual

206 native-like secondary structural elements are maintained in the unfolded state. The thermostability profile for

207 DsbB in nanodiscs compared to detergent micelles revealed two distinct differences – (**i**) the thermostability for

208 DsbB in a nanodisc is significantly higher than under micelle conditions and (**ii**) the distinct three-state/biphasic

209 unfolding model of DsbB in a nanodisc switches to a two-state/monophasic process under micelle conditions

210 revealing a major thermal transition state. These observations further signify the impact and role lipids play in

211 the thermal stability and thermal unfolding of membrane proteins.

212   The decrease in thermal stability for detergent-solubilized DsbB in micelles compared to DsbB

213 reconstituted in nanodiscs is not surprising. It is well-recognized that the function and stability of membrane

214 proteins are compromised during isolation from the membrane and delipidation through detergent solubilization

215 and even more, can be restored by reconstituting the protein back into a lipid-based model membrane system.

216 For example, the light-harvesting chlorophyll *a/b* complex (LHCIIb) of photosystem (PS) II was reported to have

217 a lower thermostability in DDM micelles (T_m = 59.4 °C) and when reconstituted in proteoliposomes, increased to

218   T_m values as high as 74.9 °C in the presence of monogalactosyl diacylglycerol (MGDG) lipids[23]. Notably, the

219   thermal stability for LHCllb was determined over a range of lipid compositions and revealed that specific lipid

220   types can shift the T_m value as much as 15 °C (i.e., phosphatidylglycerol vs. MGDG)[23]. Thermograms for the

221   Na,K-ATPase cation transporter reconstituted in DPPC (dipalmitoylphosphatidylcholine) and DPPE

222   (dipalmitoylphosphatidylethanolamine) proteoliposomes revealed different thermostability profiles under varying

223   concentrations of cholesterol suggesting that the mechanism by which the protein thermally unfolds is dependent

224   on cholesterol content[24].

225   The three-state/biphasic unfolding model of DsbB in a nanodisc is consistent with prior observations of

226   the folding/unfolding of DsbB in mixed micelles measured by stopped-flow kinetic experiments[20,25]. Although

227   thermal denaturation of membrane proteins is known to be an irreversible process, and thus true ΔG values

228   cannot be extrapolated from this data, we utilized the two-state/monophasic fitting model in MoltenProt to

229   calculate an estimated value of 3.8 ± 0.1 kcal/mol for DsbB in DM detergent micelles. We used this as a point of

230   comparison to prior kinetic studies of DsbB where they determine a true ΔG value in DM detergent micelles of

231   4.2 ± 1.4 kcal/mol. However, in our studies, detergent-solubilized DsbB in DM micelles appears to exhibit a two-

232   state/monophasic thermal unfolding behavior with a major transition in contrast to the three-state/biphasic

233   unfolding reported by Otzen *et al*. There is a second less-defined peak that occurs 40 °C post the first thermal

234   transition and is discussed further below. Furthermore, we observe this same behavior in the case of LMNG and

235   LDAO micelles (see – **Figure S3C and Figure S3E)**. In one published study, the erythropoietin-producing

236   hepatocellular carcinoma B receptor (EphB) kinase domains were investigated by thermal unfolding and

237   chemical denaturation experiments and similarly, the authors also observed a two-state/monophasic and three-

238   state/biphasic unfolding behavior for each respective method[26]. One potential explanation for these unfolding

239   mechanism differences is that thermal denaturation experiments are prone to irreversible aggregation whereas

240   chemical denaturation with urea is reversible and does not involve protein aggregation.

241   To deconvolute the second observed peak for DsbB under DM, LMNG, and LDAO conditions we

242   evaluated the dynamic light scattering (DLS) traces collected in parallel with the fluorescence measurements

243   (**Figure S3A-E**), which present several interesting observations. First, the cumulative radius plots for DsbB in

244   DM, LMNG, and LDAO each show a significant increase in system size (i.e., >4000 nm) towards the end of the

245   thermal gradient. This corresponds to the second less-defined peaks in the first derivative plots. This suggests

246   that the delay in the onset between the first and second peaks is the result of protein aggregation and micelle

247   dissociation from the unfolded protein state. Second, the cumulative radius plots for DsbB in detergent micelles

248   show marked variability. DM, LMNG, and LDAO have similar readouts with a drastic increase in system size at

249   the end of the thermal gradient. In contrast, DDM and LMPG both show a minimal increase in the cumulative

250   radius at the end of the thermal ramp. We speculate the different patterns observed for the change in system

251   size are attributed to the different chemical and physical properties of the detergent micelles. For example, DsbB

252   has a +4 charge state at the pH of our measurements, and detergents such as LMPG are negatively charged[27].

253   We propose that electrostatic interactions between LMNG and DsbB are strong enough to prevent micelle
254   dissociation from the unfolded state and thus, prevent aggregation.

255   In the case of DsbB in a dark nanodisc, the cumulative radius plot in **Figure S2A (third row)** shows that
256   the system size increases moderately to 340 nm at a temperature of 76.5 °C and 664 nm at a temperature of
257   83.9 °C. These temperature-dependent changes in cumulative radius occur after the minor and major thermal
258   unfolding states observed for DsbB. This information suggests that (i) the change in system size correlates with
259   the unfolding of DsbB and/or (ii) protein unfolding at the midpoint melting temperatures is followed by protein
260   aggregation.

261

262   **The periplasmic loops and transmembrane domain regions of DsbB reconstituted in a nanodisc unfold**
263   **as a cooperative unit along the thermal gradient.**

264   The experimental derivative plot for the unfolding curve of *dark loop* DsbB in a dark nanodisc revealed
265   two inflection points at 85.3 °C and 91.7 °C, which are in close range and above the melting temperature
266   observed for the empty fluorescent nanodisc (i.e., 86.6 °C). Despite the apparent increase in melting
267   temperature, the *dark loop* construct still exhibits a three-state/biphasic unfolding pattern suggesting that DsbB
268   unfolds as a cooperative unit. To determine if the apparent increase in stability of the *dark loop* DsbB construct
269   compared to the wt construct was due to a stabilizing effect of the *dark loop* mutations, we performed Rosetta
270   calculations on a DsbB NMR ensemble to estimate the relative energy between the two constructs. We found
271   no statistically significant difference between wt and *dark loop* DsbB energy in terms of Rosetta Energy Units
272   (REU) (**Figure S6**). This suggests that the *dark loop* mutations do not stabilize the structure enthalpically.
273   Although outside the scope of this work, another potential explanation for this increase in thermal stability for the
274   *dark loop* construct could be that we expressed it in nutrient-rich Luria-Bertani (LB) media as opposed to minimal
275   (M9) media in order to obtain enough protein yield for nanodisc reconstitutions. LB media is known to be higher
276   in ubiquinone content due to the presence of additional precursors required for synthesis[28] and ubiquinone is
277   known to bind and structurally stabilize DsbB[29]. It is also possible that interactions between the engineered Phe
278   residues and lipids in the nanodisc caused a shift in the melting temperatures and enhanced stability.

279

280   **Lipid-mediated interactions between the catalytically conserved cysteine residues of DsbB and the dark**
281   **nanodisc drive the biphasic unfolding mechanism.**

282   Time-resolved kinetic experiments showed the stability of DsbB in mixed micelles was reduced by half
283   upon the reduction of the two periplasmic disulfide bonds between residues C41-C44 and C104-C130[20]. Disulfide
284   bonds have been shown to play key roles in membrane protein stability for a number of systems such as G
285   protein-coupled receptors (GPCRs)[30] and ATP-binding cassette (ABC) transporters[31]. For example, a simulated
286   thermal unfolding of the GPCR rhodopsin revealed that the C110–C187 disulfide bond is key to retinal binding
287   and stabilizing the folded state of rhodopsin[30]. In another example, the intramolecular disulfide bond C592–C608
288   located in the extracellular loop of the ABC transporter ABCG2 was shown to be critical for protein stability (i.e.,

plasma localization and expression levels), which was significantly reduced when this disulfide bond was mutated out with glycine residues[31].

Prior studies have investigated disulfide bond interactions in the presence of lipids that contribute to the stability of proteins. For example, a Raman spectroscopy study of a lung surfactant peptide B co-solubilized in a lipid mixture of dipalmitoyl phosphatidylcholine (DPPC) and PG1,2-dioleoyl-sn-glycero-3-phospho-(1'-rac-glycerol) (DOPG) at a 4:1 lipid to protein ratio suggests that the presence of lipids "locks" the disulfide bond into a distinct conformation[32]. Furthermore, molecular dynamics (MD) simulations have investigated the role of particular disulfide bonds in the mechanism of DsbB as a disulfide bond formation mediator[33]. These MD simulations reveal that DsbB undergoes several disulfide bond rearrangements resulting in conformational changes in the periplasmic loop region. Specifically, the loop adopts a compact conformation to accommodate the C41-C130 disulfide bond. This suggests that under reducing conditions, DsbB cannot adopt this compact conformation in the periplasmic loop region, leading to a lack of stabilization and loss of the intermediate state. Furthermore, the intermediate state is only observed under lipid nanodisc conditions, suggesting that lipid-mediated interactions between the cysteine residues drive the three-state/biphasic thermal unfolding pattern.

In this work, the construct used has a disulfide bond between residues C41 and C130 and is referred to as the interloop disulfide-bond intermediate state. We find that under reducing conditions (2 mM TCEP), the thermal unfolding pattern for DsbB shifts to a two-state model and a loss of the first minor thermal transition as shown in **Figure 4B** (i.e., T_{m1} = 70.5 °C). We show that the second major thermal transition state (T_{m2}) is maintained under reduced conditions. From these results, we conclude that (i) the interloop disulfide bond plays a critical role in the thermal unfolding of DsbB and (ii) the presence of lipids contributes to the observed minor thermal transition state as this is not observed under detergent conditions. In summary, this suggests that the disulfide bond formed between the catalytically conserved cysteine residues contributes to the stabilization of a metastable intermediate state during the thermal unfolding of DsbB.

Outlook

Overall, the method developed herein will be broadly applicable in membrane protein biophysics research. It provides a simple tool to dissect the effect of lipid-protein interactions on membrane protein thermostability – interactions that are typically missed or difficult to measure using existing methods. For example, genetic mutations lead to the loss of important intermolecular interactions that cause structural instability and misfolding of proteins. This leads to serious genetic diseases such as cystic fibrosis (CF), long QT syndrome, and Charcot-Marie tooth disease. Specifically, these diseases are caused by the misfolding of an integral membrane protein including the CF transmembrane conductance regulator (CFTR)[34], the KCNQ1 ion channel[35], and the peripheral myelin protein 22 (PMP22)[36], respectively. In such cases, mutations compromise membrane protein stability, resulting in aberrant protein function. Experimental and high-throughput measurements are key for understanding (i) the effects of genetic mutations on the thermostability of membrane proteins and (ii) how mutations reshape native lipid-protein interactions to drive disease states, which have been

325   historically underappreciated[37,38]. Furthermore, our method will be used to test membrane protein design

326   candidates in cases where the goal is to design a more thermostable protein to facilitate biochemical or structural

327   studies.

328

329

330

331

332

333

334

335

336

337

338

339

340

341

342

343

344

345

346

347

348

349

350

351

352

353

354

355

356

357

358 **Figures and Tables**

359 **Figure 1**
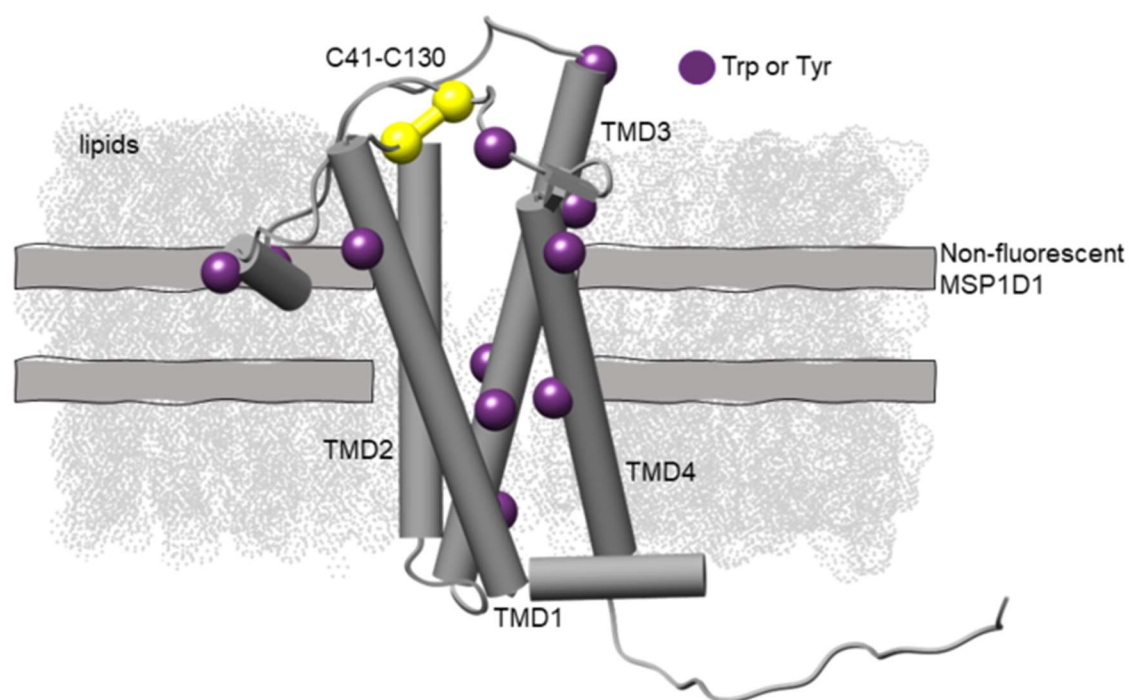
360

361 **Figure 1. The structural topology and location of the tryptophan and tyrosine residues mapped onto the**
362 **NMR-derived model of DsbB reconstituted in a dark nanodisc (PDB ID 2K73).** DsbB is reconstituted in a
363 dark nanodisc system loaded with DMPC and DMPG lipids at a 3:2 molar ratio and the non-fluorescent MSP.
364 The four transmembrane domains are labeled as TMD1-TMD4 and the interloop disulfide bond C41-C130 is
365 shown in yellow. The C41-C130 interloop disulfide bond connects the two periplasmic loops. We also show the
366 tryptophan and tyrosine residues as purple spheres for visualization.

367

368

369

370

371

372

373

374

375

376

377

378

379
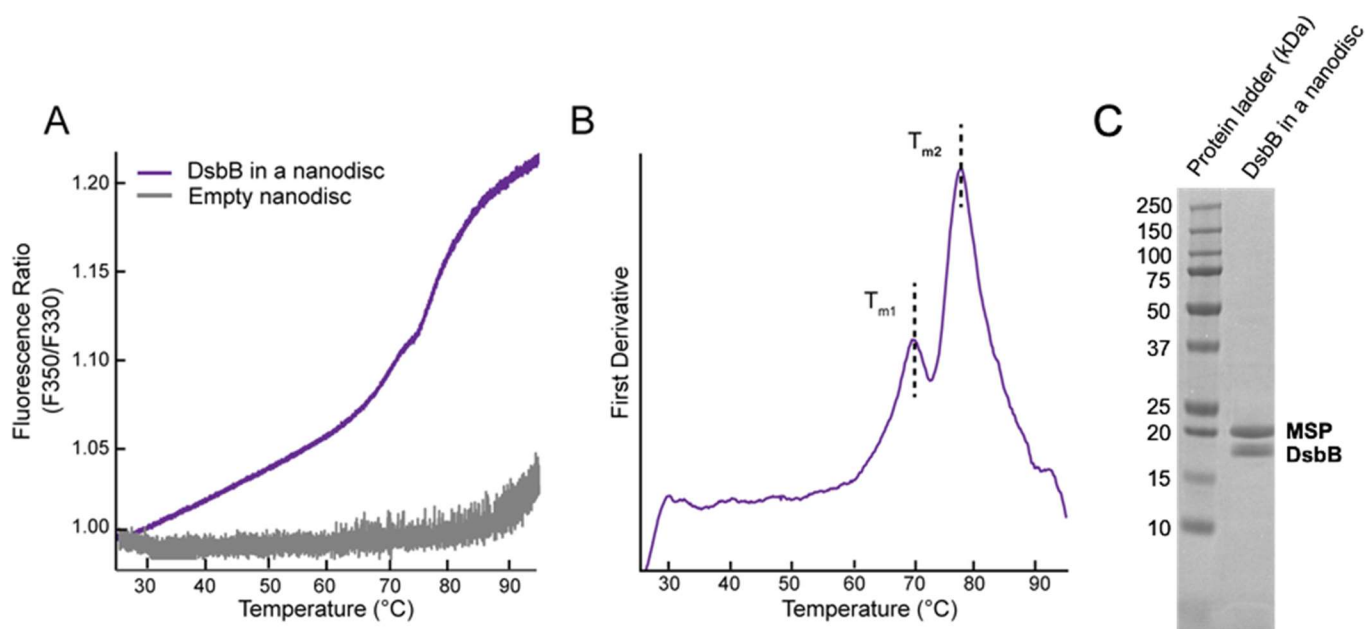
11

Figure 2

Figure 2. NanoDSF thermal unfolding curve for DsbB in a dark nanodisc. (**A**) The F350/F330 thermal unfolding curve for DsbB reconstituted in a dark nanodisc model membrane system (violet). The thermal unfolding curve for empty dark nanodiscs is shown in grey. (**B**) The first derivative plot of the F350/F330 ratio with respect to temperature for DsbB in a nanodisc. The inflection points correspond to T_m values of 70.5 °C and 77.5 °C, respectively. All samples were run in triplicate for three independent preparations and the average is plotted. (**C**) Representative SDS-PAGE gel following size exclusion to showcase the successful reconstitution of DsbB in a dark nanodisc.

12

404 **Figure 3**
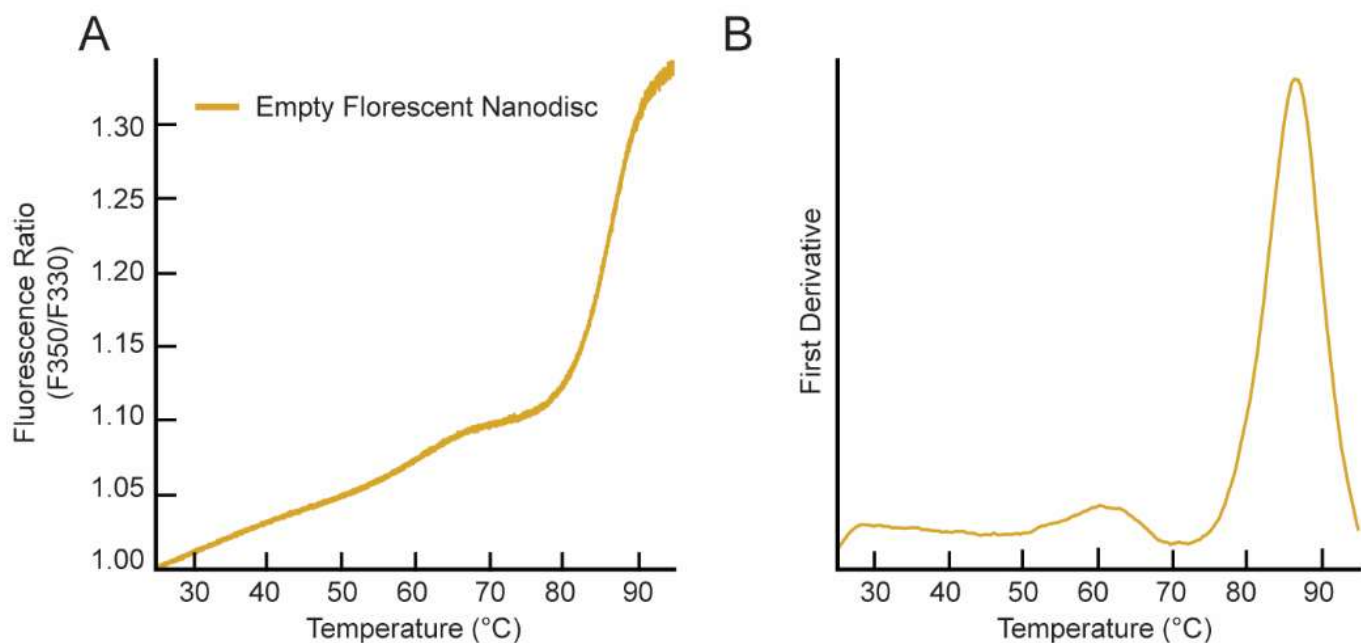
405

406 **Figure 3. NanoDSF measurement for the empty fluorescent MSP-based nanodisc.** (**A**) The F350/F330
407 thermal unfolding curve for the empty fluorescent MSP-based nanodisc. (**B**) The first derivative plot of the
408 unfolding curve shows an inflection point at a T_m value of 86.6 ± 0.6 °C. All samples were run in triplicate and
409 the average is plotted.

410

411

412

413

414

415

416

417

418

419

420

421

422

423

424

425

426

427
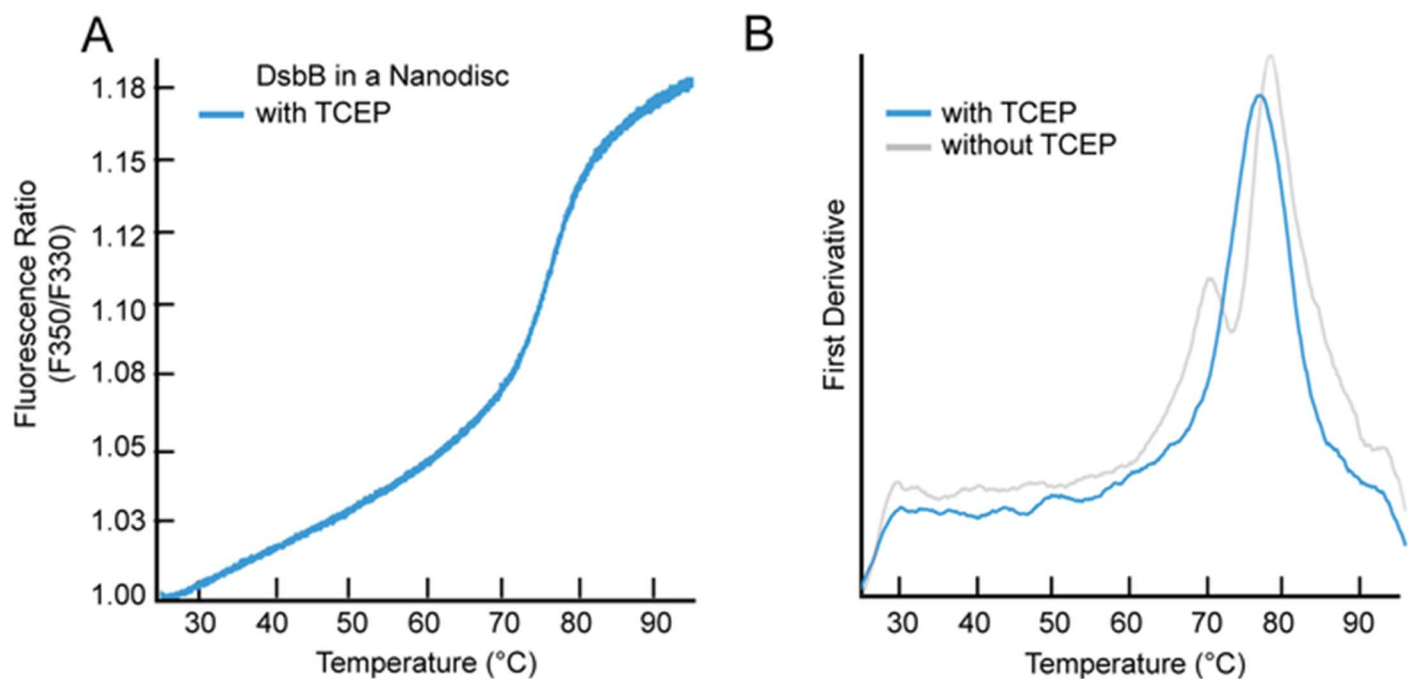
Figure 4

Figure 4. NanoDSF measurements for DsbB reconstituted in dark nanodiscs under reducing conditions. (**A**) The F350/F330 thermal unfolding curve of DsbB reconstituted in the dark nanodisc in the presence of the reducing agent TCEP at 2 mM. (**B**) The first derivative plot shows a single inflection point corresponding to a T_m value of 76.6 ± 0.5 °C. The first derivative plot for DsbB reconstituted in the dark nanodisc in the absence of reducing conditions has been overlayed as a comparison. All samples were run in triplicate and the average is plotted.

451 **Figure 5**
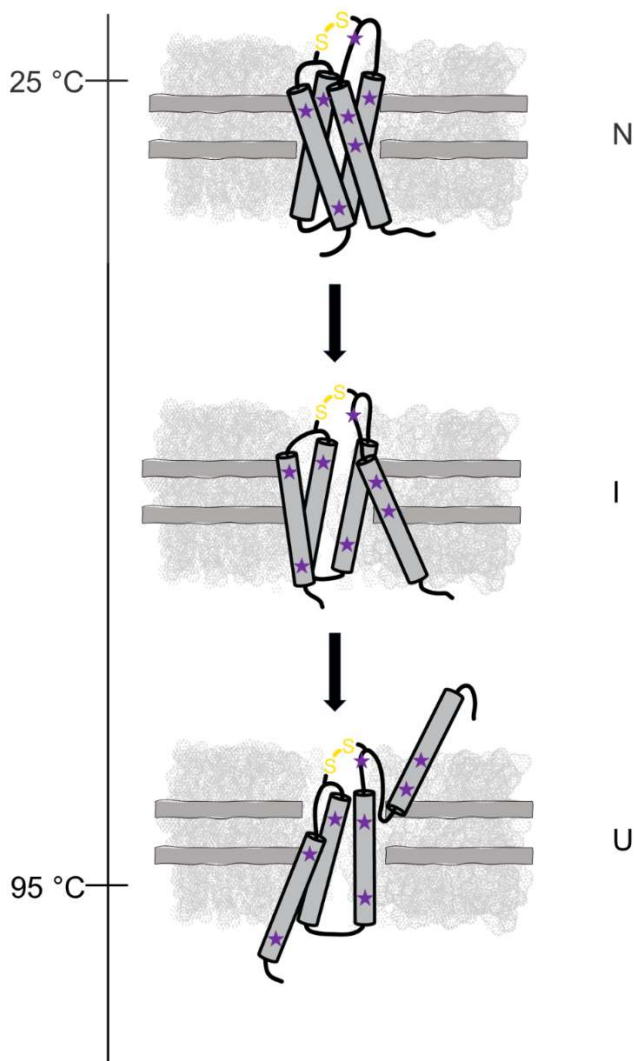
452

453 **Figure 5. Schematic summarizing the proposed three-state unfolding model for DsbB in a dark nanodisc.**

454 DsbB reconstituted in a dark nanodisc system loaded with DMPC and DMPG lipids at a 3:2 molar ratio and the

455 non-fluorescent MSP as it thermally unfolds from the native state (**N**) to an intermediate state (**I**) and to the

456 unfolded state (**U**). We propose that the three-state/biphasic model is the result of a disulfide-bond mediated

457 intermediate state in the presence of lipids. DsbB is shown in dark grey, the dark nanodisc system is shown in

458 light grey, the tryptophan and tyrosine residues are shown as purple spheres, and the C41-C130 interloop

459 disulfide bond is shown in yellow.

460

461

462

463

464

465

References

1. Carra, J.H., Murphy, E.C. & Privalov, P.L. Thermodynamic effects of mutations on the denaturation of T4 lysozyme. *Biophysical journal* **71**, 1994-2001 (1996).

2. Ibarra-Molero, B., Loladze, V.V., Makhatadze, G.I. & Sanchez-Ruiz, J.M. Thermal versus guanidine-induced unfolding of ubiquitin. An analysis in terms of the contributions from charge− charge interactions to protein stability. *Biochemistry* **38**, 8138-8149 (1999).

3. Woods, H. et al. Computational modeling and prediction of deletion mutants. *Structure* (2023).

4. Kurauskas, V. et al. How Detergent Impacts Membrane Proteins: Atomic-Level Views of Mitochondrial Carriers in Dodecylphosphocholine. *J Phys Chem Lett* **9**, 933-938 (2018).

5. Bürck, J., Wadhwani, P., Fanghänel, S. & Ulrich, A.S. Oriented circular dichroism: a method to characterize membrane-active peptides in oriented lipid bilayers. *Accounts of chemical research* **49**, 184-192 (2016).

6. Kulandaisamy, A., Sakthivel, R. & Gromiha, M.M. MPTherm: database for membrane protein thermodynamics for understanding folding and stability. *Briefings in Bioinformatics* **22**, 2119-2125 (2021).

7. Gonzalez Flecha, F.L. Kinetic stability of membrane proteins. *Biophys Rev* **9**, 563-572 (2017).

8. Plasencia, I. et al. Structure and stability of the spinach aquaporin SoPIP2;1 in detergent micelles and lipid membranes. *PLoS One* **6**, e14674 (2011).

9. Tol, M.B. et al. Thermal unfolding of a mammalian pentameric ligand-gated ion channel proceeds at consecutive, distinct steps. *Journal of Biological Chemistry* **288**, 5756-5769 (2013).

10. Ritchie, T.K. et al. Chapter 11 - Reconstitution of membrane proteins in phospholipid bilayer nanodiscs. *Methods Enzymol* **464**, 211-31 (2009).

11. Frauenfeld, J. et al. A saposin-lipoprotein nanoparticle system for membrane proteins. *Nat Methods* **13**, 345-51 (2016).

12. Guo, Y. Detergent-free systems for structural studies of membrane proteins. *Biochemical Society Transactions* **49**, 1361-1374 (2021).

13. Sanders, M.R., Findlay, H.E. & Booth, P.J. Lipid bilayer composition modulates the unfolding free energy of a knotted alpha-helical membrane protein. *Proc Natl Acad Sci U S A* **115**, E1799-E1808 (2018).

14. Laganowsky, A. et al. Membrane proteins bind lipids selectively to modulate their structure and function. *Nature* **510**, 172-175 (2014).

15. Nji, E., Chatzikyriakidou, Y., Landreh, M. & Drew, D. An engineered thermal-shift screen reveals specific lipid preferences of eukaryotic and prokaryotic membrane proteins. *Nat Commun* **9**, 4253 (2018).

16. Treuheit, N.A. et al. Membrane Interactions, Ligand-Dependent Dynamics, and Stability of Cytochrome P4503A4 in Lipid Nanodiscs. *Biochemistry* **55**, 1058-69 (2016).

17. Flayhan, A. et al. Saposin Lipid Nanoparticles: A Highly Versatile and Modular Tool for Membrane Protein Research. *Structure* **26**, 345-355 e5 (2018).

18. McLean, M.A., Denisov, I.G., Grinkova, Y.V. & Sligar, S.G. Dark, Ultra-Dark and Ultra-Bright Nanodiscs for membrane protein investigations. *Anal Biochem* **607**, 113860 (2020).

19. Zhou, Y. et al. NMR solution structure of the integral membrane enzyme DsbB: functional insights into DsbB-catalyzed disulfide bond formation. *Mol Cell* **31**, 896-908 (2008).

20. Otzen, D.E. Folding of DsbB in mixed micelles: a kinetic analysis of the stability of a bacterial membrane protein. *J Mol Biol* **330**, 641-9 (2003).

21. Sehgal, P. & Otzen, D.E. Thermodynamics of unfolding of an integral membrane protein in mixed micelles. *Protein Sci* **15**, 890-9 (2006).

22. Lee, A.G. Membrane lipids: it's only a phase. *Current Biology* **10**, R377-R380 (2000).

23. Yang, C., Boggasch, S., Haase, W. & Paulsen, H. Thermal stability of trimeric light-harvesting chlorophyll a/b complex (LHCIIb) in liposomes of thylakoid lipids. *Biochim Biophys Acta* **1757**, 1642-8 (2006).

24. Yoneda, J.S., Rigos, C.F., de Lourenço, T.F.A., Sebinelli, H.G. & Ciancaglini, P. Na, K-ATPase reconstituted in ternary liposome: The presence of cholesterol affects protein activity and thermal stability. *Archives of biochemistry and biophysics* **564**, 136-141 (2014).

25. Otzen, D.E. Mapping the folding pathway of the transmembrane protein DsbB by protein engineering. *Protein Eng Des Sel* **24**, 139-49 (2011).

16

26. Overman, R.C., Debreczeni, J.E., Truman, C.M., McAlister, M.S. & Attwood, T.K. Biochemical and biophysical characterization of four EphB kinase domains reveals contrasting thermodynamic, kinetic and inhibition profiles. *Biosci Rep* **33**(2013).

27. Lee, H.J., Lee, H.S., Youn, T., Byrne, B. & Chae, P.S. Impact of novel detergents on membrane protein studies. *Chem* **8**, 980-1013 (2022).

28. Kazemzadeh, K. et al. The biosynthetic pathway of ubiquinone contributes to pathogenicity of Francisella novicida. *Journal of Bacteriology* **203**, e00400-21 (2021).

29. Zhou, Y. et al. NMR solution structure of the integral membrane enzyme DsbB: functional insights into DsbB-catalyzed disulfide bond formation. *Molecular cell* **31**, 896-908 (2008).

30. Rader, A.J. et al. Identification of core amino acids stabilizing rhodopsin. *Proceedings of the National Academy of Sciences* **101**, 7246-7251 (2004).

31. Wakabayashi, K. et al. Intramolecular disulfide bond is a critical check point determining degradative fates of ATP-binding cassette (ABC) transporter ABCG2 protein. *J Biol Chem* **282**, 27841-6 (2007).

32. Biswas, N., Waring, A.J., Walther, F.J. & Dluhy, R.A. Structure and conformation of the disulfide bond in dimeric lung surfactant peptides SP-B1-25 and SP-B8-25. *Biochim Biophys Acta* **1768**, 1070-82 (2007).

33. Tang, M. et al. Structure of the disulfide bond generating membrane protein DsbB in the lipid bilayer. *Journal of molecular biology* **425**, 1670-1682 (2013).

34. McDonald, E.F. et al. Structural Comparative Modeling of Multi-Domain F508del CFTR. *Biomolecules* **12**(2022).

35. Kuenze, G. et al. Allosteric mechanism for KCNE1 modulation of KCNQ1 potassium channel activation. *Elife* **9**(2020).

36. Marinko, J.T. et al. Glycosylation limits forward trafficking of the tetraspan membrane protein PMP22. *J Biol Chem* **296**, 100719 (2021).

37. Levental, I. & Lyman, E. Regulation of membrane protein structure and function by their lipid nano-environment. *Nature Reviews Molecular Cell Biology*, 1-16 (2022).

38. Marx, D.C. & Fleming, K.G. Membrane proteins enter the fold. *Curr Opin Struct Biol* **69**, 124-130 (2021).

39. Nasr, M.L. et al. Covalently circularized nanodiscs for studying membrane proteins and viral entry. *Nature methods* **14**, 49-52 (2017).

40. Kotov, V. et al. High-throughput stability screening for detergent-solubilized membrane proteins. *Sci Rep* **9**, 10379 (2019).

41. Hunter, J.D. Matplotlib: A 2D graphics environment. *Computing in science & engineering* **9**, 90-95 (2007).

42. Kotov, V. et al. In-depth interrogation of protein thermal unfolding data with MoltenProt. *Protein Science* **30**, 201-217 (2021).

43. McDonald, E.F., Jones, T., Plate, L., Meiler, J. & Gulsevin, A. Benchmarking AlphaFold2 on peptide structure prediction. *Structure* **31**, 111-119. e2 (2023).

44. Yarov-Yarovoy, V., Schonbrun, J. & Baker, D. Multipass membrane protein structure prediction using Rosetta. *Proteins: Structure, Function, and Bioinformatics* **62**, 1010-1025 (2006).

Acknowledgments

Author Contributions

Conceptualization, KVL. Data curation, JAS and JRM; Formal analysis, JAS, JRM, KVL; Funding acquisition, JM; Investigation, JAS, JRM, EFM, KVL; Methodology, KVL; Supervision, KVL and JM.; Writing—original draft, JAS and EFM; Writing—review and editing, EFM, JM, and KVL. All authors have read and agreed to the published version of the manuscript.

Competing Interests

The authors declare no competing interests.

Methods

Expression and purification of the non-fluorescent membrane scaffold protein (MSP1D1) and fluorescent MSP1D1 construct. The non-fluorescent and fluorescent MSP1D1 protein genes were cloned in a pET28a vector containing a tobacco etch virus (TEV) protease-cleavable N-terminal His$_6$ tag. BL21(DE3) competent *E. coli* cells were transformed with the target plasmid and grown on Luria-Bertani (LB) agar plates overnight at 37 °C. A single colony was selected and used to inoculate a 150 mL LB starter culture and grown overnight at 37 °C. Flasks containing 1L of terrific broth (TB) media were inoculated with 10 mL of the starter culture and grown at 37 °C at 230 rpm in the presence of 100 ng/ml kanamycin. Protein expression was induced at an OD$_{600}$ of 0.6-0.8 with 1 mM IPTG (isopropyl β-D-1-thiogalactopyranoside) and cultured for another 24 hours at 20 ºC. Cells were harvested by centrifugation at 6500 rpm for 20 minutes and cell pellets were stored at -80 ºC or immediately resuspended in lysis buffer for purification.

Cell pellets expressing the non-fluorescent or fluorescent MSP1D1 proteins were resuspended (5 mL/gram of pellet) in Buffer A (50 mM Tris, 300 mM NaCl, pH 8.0) with the addition of 1 mM PMSF, 1% Triton X-100, EDTA-free protease cocktail inhibitor tablet (Sigma-Aldrich) (1 tablet/per 50 mL of buffer), and 5 mM Mg acetate. The cells were lysed by sonication for 10 minutes (60% amplitude with 5 seconds on/5 seconds off) on ice. The cell lysis solution was centrifuged at 50,000 x g for 20 minutes and the supernatant was loaded onto a Ni-NTA gravity-flow column. The Ni-NTA resin was washed with 10 column volumes of the following in this order: Buffer A and 1% Triton X-100, Buffer A and 75 mM sodium cholate, Buffer A, and Buffer A plus 20 mM imidazole. Proteins were eluted with Buffer A containing 500 mM imidazole. Isolated proteins were dialyzed against TEV cleavage buffer (20 mM Tris-HCl, 100 mM NaCl, 1 mM DTT, pH 7.5) at 4 ºC for 24 hours. The TEV cleavage reaction was set up using TEV protease at a 1:50 ratio of protease to protein to remove the N-terminal His$_6$ tag.

The cleaved sample was loaded onto a second Ni-NTA column to remove the TEV protease and N-terminal His$_6$ tag. The flow-through was collected containing the target protein. The MSP1D1 samples were size excluded using a 120 mL HiLoad® 16/600 Superdex® S200 preparative column (Cytiva) equilibrated with reconstitution buffer (40 mM Tris-HCl, 200 mM NaCl, pH 7.5). Protein fractions were analyzed by SDS-PAGE. Pooled fractions were quantified using a Bradford assay and concentrated to 500 µM in an Amicon centrifugal filter (10,000 MWCO) and analyzed by SDS-PAGE to confirm the purity of the samples were greater than 95%. As a control, the Ni-NTA bound TEV protease and His$_6$ tag were eluted from the resin. The resin was washed with reconstitution buffer followed by a 10 mM imidazole wash. The TEV protease and cleaved His$_6$ tag were eluted with reconstitution buffer and 500 mM imidazole.

Expression and purification of DsbB. The "wild-type" (wt) DsbB protein construct[29] was inserted into pET22b vector and transformed into BL21(DE3) *E. coli* cells. Cells were grown on Luria-Bertani (LB) agar plates containing 100 µg/mL ampicillin overnight at 37 ºC. A single colony was selected and used to inoculate a 150

19

636 mL starter culture grown overnight at 37 ºC. Flasks containing 1L of minimal (M9) media were inoculated with

637 10 mL of starter culture and grown in the presence of 100 µg/mL ampicillin. Cells were cultured at 37 °C at 230

638 rpm until the OD_{600} reached 0.6-0.8. Cells were transferred to room temperature and protein expression was

639 induced with 1 mM IPTG for 18 hours. Cells were harvested by centrifugation at 6500 rpm for 15 minutes at 4

640 ºC. Cell pellets were stored at -80 ºC or immediately resuspended in lysis buffer for purification.

641

642 Each cell pellet was resuspended in 40 mL of Buffer B (50 mM Tris-HCl, 300 mM NaCl, pH 8.0) with the addition

643 of 1 mM PMSF, 5 mM Mg Acetate, and 1 EDTA-free protease cocktail inhibitor tablet (Sigma-Aldrich) (1 tablet/per

644 50 mL of buffer). The cell lysis solution was rotated at 4 °C for 30 minutes and then lysed by sonication for 10

645 minutes (60% amplitude with 5 seconds on/5 seconds off). The membrane fraction was pelleted by

646 ultracentrifugation at 100,000 x g for 1 hour at 4 °C and the supernatant was discarded. The membrane fraction

647 was homogenized on ice with Buffer B (20 mL/pellet) containing 1% dodecylphosphocholine (DPC, FOS-

648 CHOLINE-12, Anatrace). Homogenized cells were ultracentrifuged at 100,000 x g for 30 minutes to remove the

649 insoluble fraction. The remaining supernatant was loaded onto a Ni-NTA gravity-flow column equilibrated with

650 Buffer B and 0.05% DPC. The Ni-NTA column was washed with Buffer B and 0.05% DPC followed by Buffer B

651 plus 0.05% DPC and 10 mM imidazole. DsbB was eluted with Buffer B plus 0.05% DPC and 500 mM imidazole.

652 The collected sample was concentrated to 500 µM and size excluded using a 120 mL HiLoad® 16/600

653 Superdex® S200 preparative column (Cytiva) equilibrated with FPLC buffer (50 mM Tris-HCl, 300 mM NaCl,

654 0.15% DPC, pH 8.0). The pooled fractions were concentrated to 500 µM in an Amicon centrifugal filter (10,000

655 MWCO) and analyzed by SDS-PAGE to confirm the purity of the sample was greater than 95%. For the reduced

656 DsbB sample, we followed the above protocol with the exception that each buffer in the purification protocol was

657 supplemented with 2 mM TCEP.

658

659 ***Dark loop* DsbB mutagenesis, expression, and purification.** A modified DsbB protein construct containing

660 mutations W113F, W119F, and W135F was engineered and inserted into a pET22b vector. The plasmid was

661 transformed into BL21(DE3) *E. coli* cells and expressed and purified following the same protocol as described

662 for wt DsbB. The protein yield for this construct was low. To increase the protein yield of this *dark loop* construct

663 we performed a multiple sequence alignment (MSA) and identified that residue W119 is highly conserved. For

664 this reason, we engineered a second construct with a W119L mutation in place of the W119F mutation using

665 site-directed mutagenesis. This MSA-modified construct containing mutations W113F, W119L, and W135F was

666 transformed into C43(DE3) *E. coli* cells and expressed in LB media to optimize the expression of the *dark loop*

667 construct. Flasks containing 1L of LB media were inoculated with 10 mL of starter culture and grown in the

668 presence of 100 µg/mL ampicillin. Cells were cultured at 37 °C at 230 rpm until the OD_{600} reached 0.6-0.8 and

669 protein expression was induced with 1 mM IPTG for 5 hours at 37 °C. The purification of *dark loop* DsbB followed

670 the same protocol as described above for wt DsbB.

671

672 **Reconstitution reactions for DsbB in dark nanodiscs and reconstitution reactions for empty nanodiscs.**

673 All purified proteins were concentrated to 500 µM as described above and reconstitutions were set up as

674 previously described by Nasr. *et al*[39]. Lipids were prepared as an 80 mM stock of DMPC and DMPG lipids at a

675 3:2 molar ratio solubilized in 10% DM. Bio-beads SM2 resin (Bio-Rad) was prepared freshly prior to each reaction

676 by washing the beads with 10 mL of methanol followed by excess deionized water. DsbB was assembled into

677 dark nanodiscs by adding DsbB (160 µM), non-fluorescent MSP1D1 (160 µM), and lipids (13.6 mM) to

678 reconstitution buffer at a 1:1:85 ratio, respectively. Reaction components were added to the reconstitution buffer

679 in the order of lipids, MSP1D1, and DsbB. The reaction was then equilibrated at room temperature for 1 hour.

680 Fresh Bio-beads (0.5g of wet beads/300 µl of total reaction volume) were added to the reaction and allowed to

681 tumble overnight at room temperature to remove all detergents. The DsbB-containing nanodisc solution was

682 collected to remove the Bio-beads and loaded three times onto a Ni-NTA column equilibrated with reconstitution

683 buffer (i.e., DsbB is His$_6$-tagged). The Ni-NTA resin was washed with excess reconstitution buffer to remove empty

684 nanodiscs and/or large vesicles. The assembled DsbB-nanodisc complex was then size excluded at room

685 temperature using a 24 mL Superdex® 200 Increase 10/300 GL column (Cytiva) equilibrated with reconstitution

686 buffer. Selected fractions were analyzed by SDS-PAGE to confirm the purity of the DsbB-nanodisc samples.

687 Fractions were pooled and concentrated at room temperature using a low spin speed (i.e., 2500 x g) in an Amicon

688 centrifugal filter (30,000 MWCO) to 1 mg/ml. Empty nanodisc reconstitution reactions were performed using the

689 same protocol described above with the exception that the volume of DsbB was replaced with reconstitution buffer

690 (i.e., the reaction volumes were the same for each reconstitution). Reduced DsbB was assembled into nanodiscs

691 as described above with the exception that the reconstitution buffer was supplemented with 2 mM TCEP.

692

693 **Preparing detergent-solubilized DsbB under different micelle conditions for nanoDSF measurements.** To

694 prepare DsbB under different detergent micelle conditions, we followed the method outlined for a membrane

695 protein stability detergent screen as described[40]. Briefly, DPC-solubilized DsbB was diluted 10-fold into detergent

696 buffers (DDM, DM, LDAO, LMPG, and LMNG) that were made with a 50-fold excess of the critical micelle

697 concentration (CMC) of the target detergent. The diluted DsbB samples were incubated at 4 °C overnight to

698 ensure detergents were fully exchanged. All detergent micelle samples were prepared to a final concentration of

699 1 mg/mL.

700

701 **NanoDSF thermostability measurements.** All samples were run on a Prometheus NT.48 nanoDSF instrument

702 (NanoTemper Technologies). Samples were set up in triplicate at a final concentration of 1 mg/mL (10

703 µL/capillary). The *dark loop* DsbB nanodisc sample was run in triplicate at a final concentration of 2 mg/mL to

704 optimize the signal readout. All nanodisc samples and detergent samples were measured at a scan rate of 0.1

705 °C per minute over a temperature range of 25 °C to 95 °C and 20 °C to 95 °C, respectively. Samples were

706 excited at 280 nm and the intrinsic tryptophan fluorescence at 350 nm and 330 nm were recorded as a function

707 of temperature to monitor changes upon thermal unfolding.

708

709   **Data analysis**. All raw nanoDSF data was collected and then exported from the Prometheus Panta Control

710   software for visualization in MoltenProt[40]. The experimental derivatives were exported from MoltenProt and

711   further analyzed in a Jupyter Notebook through Matplotlib[41]. The F350/F330 ratios for each of the triplicate

712   samples were averaged and normalized to the initial value with Matplotlib. The first derivatives were plotted with

713   Matplotlib to determine the inflection points corresponding to the melting temperatures. The fraction unfolded

714   curves were calculated and plotted by fitting the F350/F330 ratio data to a two-state equilibrium model. The rate

715   constants of the unfolding transition and baseline transition as well as the baseline offset and noise were

716   extrapolated. These parameters were utilized to calculate the baseline-corrected experimental curves from the

717   equation utilized by MoltenProt[42].

718

719   **Rosetta calculations.** DsbB (PDB ID: 2K73[29]) was broken into its 20 constituent NMR models as described

720   previously[43]. Next, each individual model was used to create a corresponding *dark loop* model by introducing

721   W113F, W119L, and W135F using the MutateResidue mover in Rosetta. Finally, the 20 wt and 20 *dark loop*

722   DsbB models were energetically minimized using FastRelax in Rosetta for one iteration and scored using a

723   membrane scoring function[44].

724

725

726

727

728

729

730

731

732

733

734

735

736

737

738

739

740

741

742

743 **Supplemental Materials**

744 **Table S1**

Experimental Condition	T_{m1} (°C)	T_{m2} (°C)
DsbB – dark nanodisc	70.5 ± 0.3 70.0 ± 0.1 70.3 ± 0.6	77.5 ± 0.1 79.1 ± 0.2 79.7 ± 0.5
empty fluorescent nanodisc	86.6 ± 0.6	
dark loop DsbB – dark nanodisc	85.3 ± 0.6	91.7 ± 0.3
DsbB – dark nanodisc + TCEP	76.6 ± 0.5	
DsbB – DDM	55.6 ± 0.2	
DsbB – LMPG	45.4 ± 0.1	
DsbB – LMNG	41.0 ± 1.2	
DsbB – DM	40.1 ± 0.9	
DsbB – LDAO	36.7 ± 0.2	

745 **Table S1. Table summarizing the measured inflection points (T_m).**

746

747

748

749

750

751

752

753

754

755

756

757

758

759

760

761

23
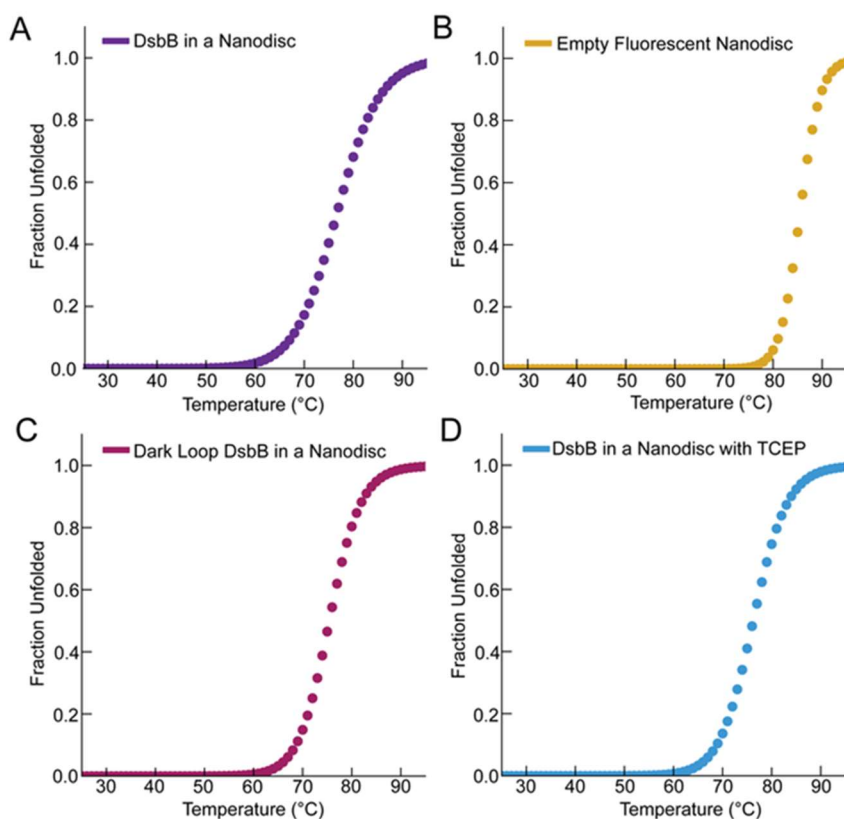
Figure S1

Figure S1. Fraction unfolded plotted as a function of temperature for the nanodisc samples evaluated in this study. For visualization, baseline-corrected experimental curves were calculated from the rate constant of the unfolding transition, the rate constant of the baseline transition, baseline noise, and baseline offset. Fraction unfolded plots are shown for (**A**) DsbB in a dark nanodisc, (**B**) empty fluorescent nanodisc, (**C**) *dark loop* DsbB in a dark nanodisc, and (**D**) DsbB in a dark nanodisc under reducing conditions.
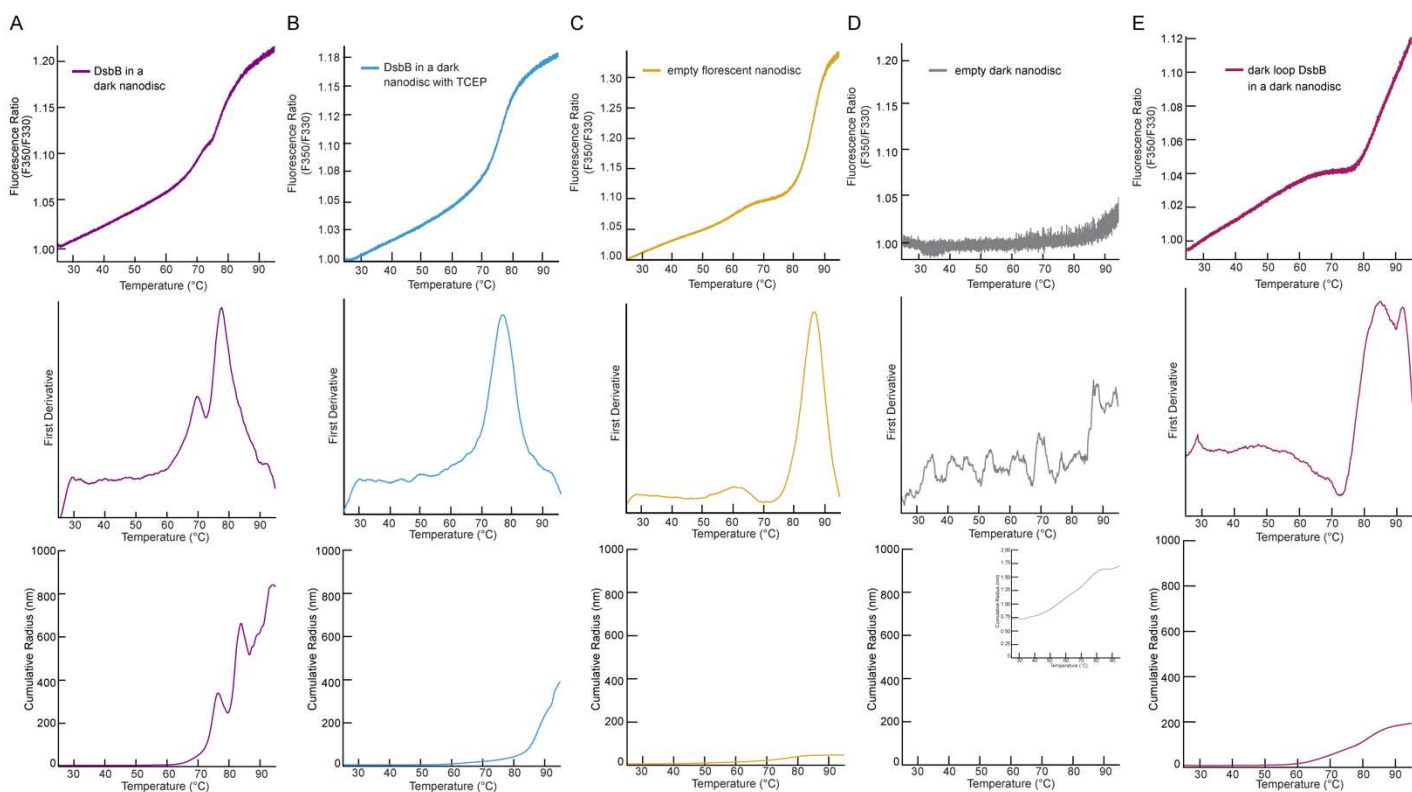
Figure S2

Figure S2. NanoDSF unfolding curves, first derivative, and cumulative radius plots for all nanodisc samples. (**A**) DsbB in a dark nanodisc, (**B**) DsbB in a dark nanodisc under reducing conditions, (**C**) empty fluorescent nanodisc, (**D**) empty dark nanodisc, and (**E**) *dark loop* DsbB in a dark nanodisc. **Top row**: The F350/F330 thermal unfolding curves for each of the nanodisc samples. **Second row**: The first derivative plots for each nanodisc sample. **Third row**: The cumulative radius plots from dynamic light scattering measurements collected in tandem with the fluorescence measurements. All samples were run in triplicate (n=3) with the exception that DsbB in a dark nanodisc was run for three independent sample preparations in triplicate (n=9), the average was plotted.
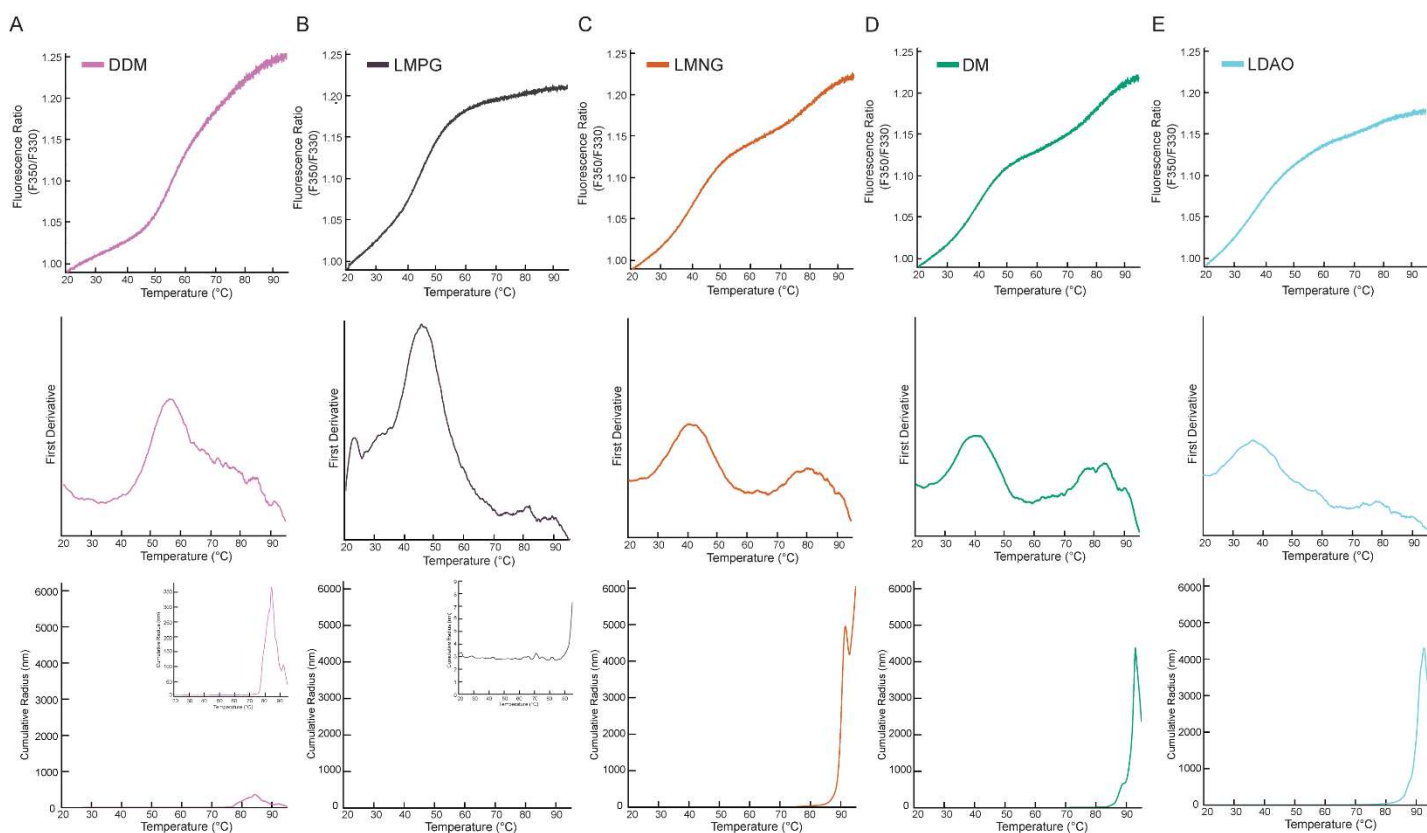
25

Figure S3

Figure S3. NanoDSF unfolding curves, first derivative, and cumulative radius plots for detergent-solubilized DsbB under a panel of micelle conditions. (**A**) DDM, (**B**) LMPG, (**C**) LMNG, (**D**) DM, and (**E**) LDAO. **Top row**: The F350/F330 thermal unfolding curves for detergent-solubilized DsbB under a panel of different micelle conditions. **Second row**: The first derivative plots for detergent-solubilized DsbB. The inflection points correspond to T_m values of 36.7 ± 0.2 °C (LDAO, cyan), 40.1 ± 0.9 °C (DM, green), 41.0 ± 1.2 °C (LMNG, orange), 45.4 ± 0.1 °C (LMPG, purple), and 55.6 ± 0.2 °C (DDM, pink). **Third row**: The cumulative radius plots from dynamic light scattering measurements collected in tandem with fluorescence measurements. All samples were run in triplicate (n=3) and the average was plotted.
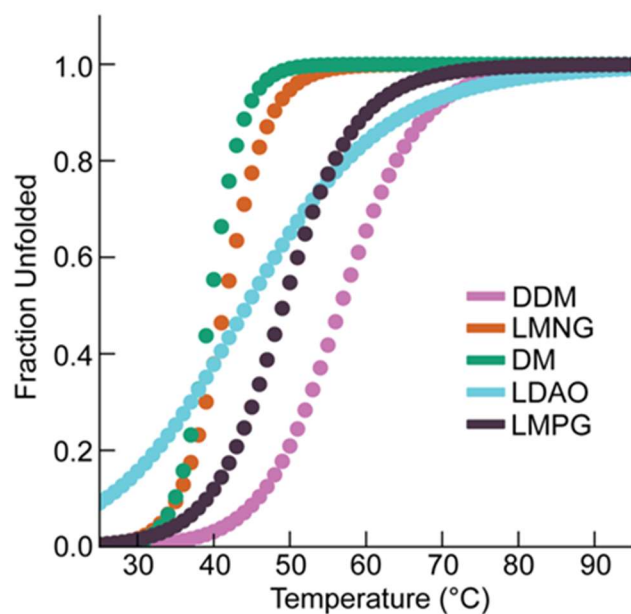
823 **Figure S4**

824

825 **Figure S4. Fraction unfolded plotted as a function of temperature for detergent-solubilized DsbB under**
826 **a panel of different detergent micelle conditions.** The fraction unfolded is plotted for DsbB under a panel of
827 different detergent micelle conditions including DDM, LMNG, DM, LDAO, and LMPG. For visualization, baseline-
828 corrected experimental curves were calculated from parameters derived after fitting the data to an equilibrium
829 two-state unfolding model in MoltenProt[42].

830

831

832

833

834

835

836

837

838

839

840

841

842

843

844

845

846
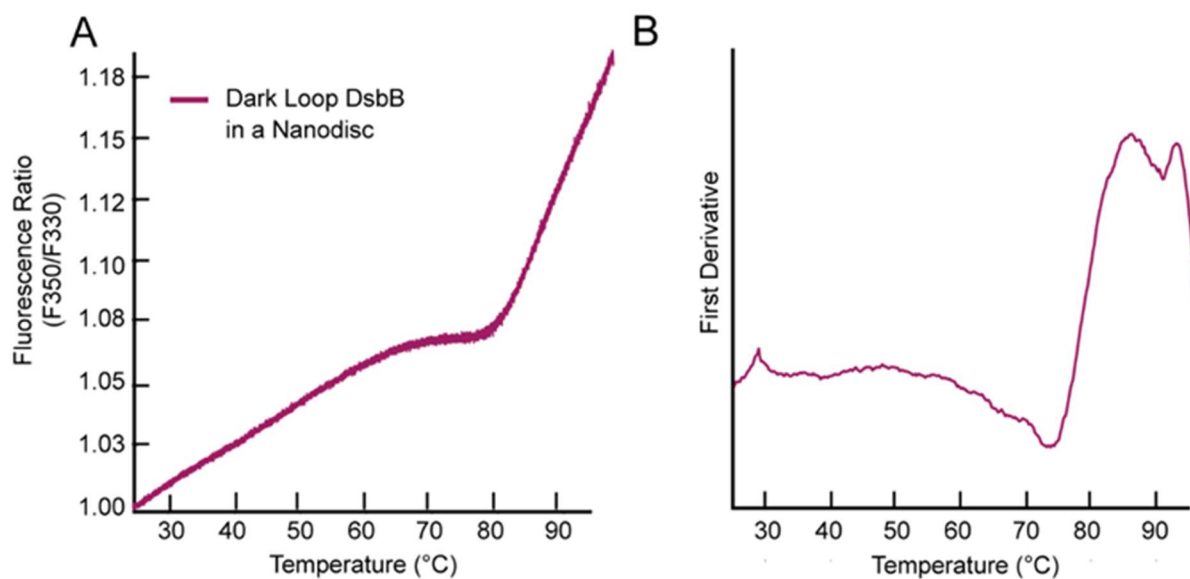
847 **Figure S5**

848

849 **Figure S5. NanoDSF thermal unfolding curve for dark loop DsbB in a dark MSP-based nanodisc.** (**A**) The

850 F350/F330 thermal unfolding cure for dark loop DsbB reconstituted in a dark nanodisc model membrane system.

851 (**B**) The first derivative plot of the F350/F330 ratio with respect to temperature for dark loop DsbB in a nanodisc.

852 The inflection points correspond to Tm values of 85.3 °C and 91.7 °C, respectively. All samples were run in

853 triplicate.

854

855

856

857

858

859

860

861

862

863

864

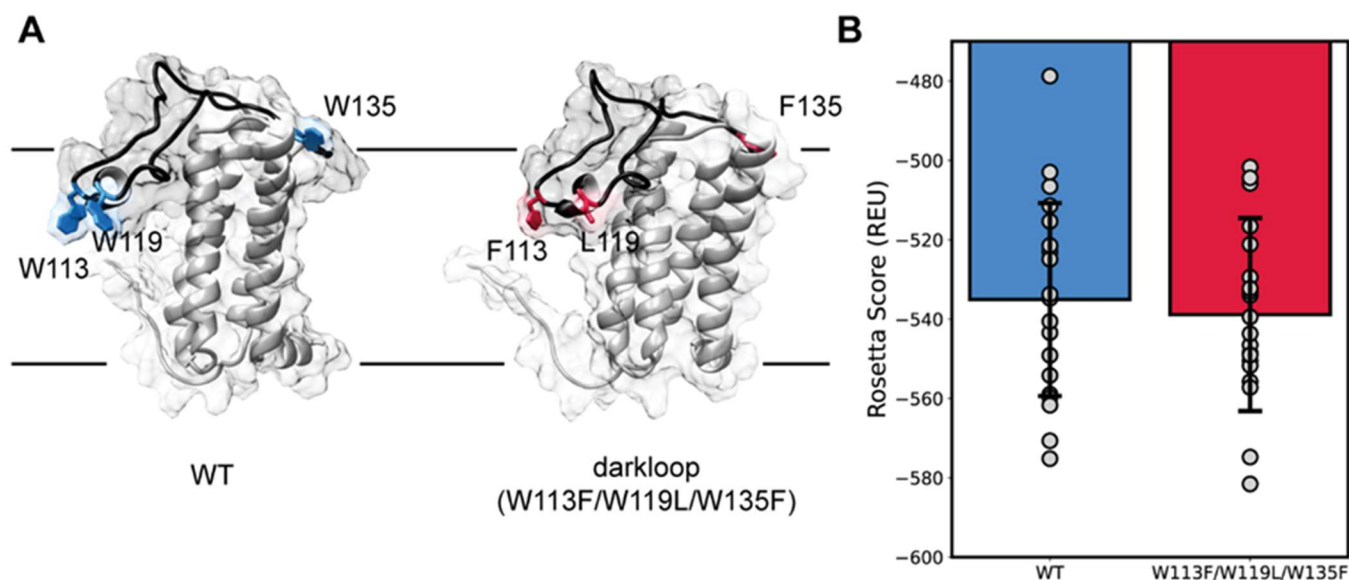865

866

867

868

869

870

871

872   **Figure S6**

873

874   **Figure S6. Rosetta calculations of wt and dark loop DsbB based on the ensemble NMR model PDB ID:**

875   **2K73.** (**A**) Illustration of the residues that were modified to generate the dark loop DsbB construct, which was

876   then relaxed and scored with a Rosetta membrane protein score function. Wt tryptophan residues are depicted

877   in blue and corresponding dark loop residues are depicted in red. The periplasmic loop is shown in black. (**B**)

878   Bar and whisker plot of the membrane score functions for both wt (blue) and dark loop (red) DsbB with a 4

879   Rosetta energy unit (REU) reduction from -535 REU in wt to -539 REU for dark loop DsbB. Grey dots represent

880   an individual model from the 20-model ensemble and error bars indicate the standard deviations of the scores.

29